

Adaptive Biomimetic Neuronal Circuit System Based on Myelin Sheath Function

Xiaosong Li, Jingru Sun, *Member, IEEE*, Wenjing Ma,
Yichuang Sun, *Senior Member, IEEE*, Chunhua Wang, Jiliang Zhang, *Senior Member, IEEE*

Abstract—Brain-inspired neuromorphic computing architectures are receiving significant attention in the consumer electronics field owing to their low power consumption, high computational capacity, and strong adaptability, where highly biomimetic circuit design is at the core of neuromorphic network research. Myelin sheaths are crucial cellular components in building stable circuits in biological neurons, capable of adaptively adjusting the conduction speed of neural signals. However, current research on neuronal circuits relies on simplified mathematical models and overlooks the adaptive functionality of myelin sheaths. This paper is based on the dynamic mechanism of myelination, utilizing physical devices such as memristors and voltage-controlled variable capacitors to simulate the physiological functions of myelin sheaths, and other organelles. Furthermore, adaptive biomimetic neuronal circuit system (ABNCS) is constructed by connecting various devices according to the physiological structure of neurons. *PSpice* simulations show that the ABNCS can adjust its parameters autonomously as the number of action potentials (APs) increase, which modifies the neuron's activation criteria and firing rate. Through circuit experiments, *PSpice* simulations were further validated. Implementing myelin sheath functions in the neuronal circuit improves adaptability and reduces power consumption, and when combined with artificial synapses to construct neural networks, can form more stable neural circuits.

Index Terms—Myelin sheath, Memristor, Neuromorphic networks, Ion channel, Neurodynamics, Biomimetic neuronal circuits.

I. INTRODUCTION

Developing intelligent, high-speed, and low-power consumer electronics has become the primary focus of the electronics industry [1], [2]. Neuromorphic networks, which emulate biological systems, are gaining attention in consumer electronics for their high speed and low power consumption [3]–[5]. As the biological foundation for the study of neuromorphic networks, cognitive neuroscience research suggests that the

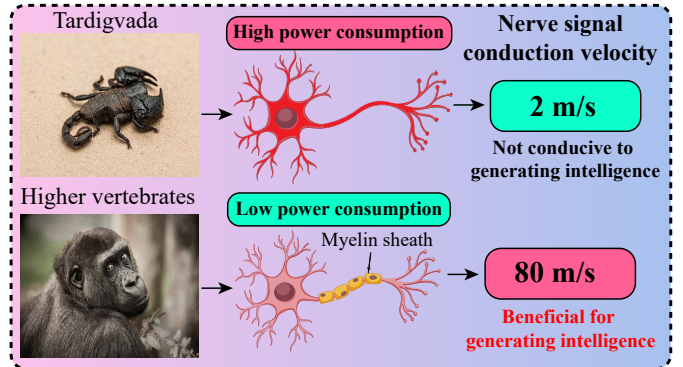


Fig. 1. Comparison of Signal Conduction Speed between Myelinated and Unmyelinated Neurons.

intrinsic computational capability and plasticity of neurons are essential foundations for performing tasks involving association, memory, and learning [6], [7], where the plasticity can be achieved through the well known synapses, in addition to, myelin sheaths [8], [9]. Myelin sheaths typically occur around the axons of neurons in vertebrates and some arthropods. Oligodendrocytes produce a substantial amount of new myelin along the axon during the growth of neurons. The formation and development of myelin sheaths are promoted by neuronal activity [10]–[12] and influence the type of axons [10], [13]. The insulation formed by myelin sheaths between neurons effectively prevents mutual interference during the process of signal transmission and increases the speed of neuronal signal transmission by several tens of times [14], [15], as shown in Fig. 1. Higher vertebrates with myelin sheaths gradually developed ultra-low power intelligence over millions of years of evolution. A certain level of intelligence and low power consumption are essential for electronic products like smartphones and smart home systems.

Myelin sheaths are crucial for neuronal activity, allowing for rapid exchange of information between brain regions, which is essential for cognitive function and human intelligence development [16]. The speed at which neurons transmit signals is the basis for all neural activity over time [17], [18]. The axon serves as the foundational conduit for high-speed transmission of neural signals [19], and its length, diameter, and myelin sheath layers directly influence the speed and duration of signal transmission [14], [20], [21]. Myelin sheaths serve as the physical foundation for the quick transmission of neural signals [22], [23]. Spike code depends on the firing rate of signals, which is influenced by stimulus intensity, synaptic plas-

Manuscript received X X, 2023.

This work is supported by the National Natural Science Foundation of China (62171182), Natural Science Foundation Project of Chongqing, Chongqing Science and Technology Commission (CSTB2022NSCQ-M SX0770), (Corresponding author: Jingru Sun)

Xiaosong Li, Jingru Sun are with the College of Computer Science and Electronic Engineering, Hunan University, Changsha 410082, China and Chongqing Research Institute, Hunan University, Chongqing 401120, China. E-mail: liguangbi@hnu.edu.cn, jt_sunjr@hnu.edu.cn.

Wenjing Ma, Chunhua Wang are with the College of Computer Science and Electronic Engineering, Hunan University, Changsha 410082, China. E-mail: cx_mwj@hnu.edu.cn, wch1227164@hnu.edu.cn.

Yichuang Sun is with the School of Engineering and Computer Science, University of Hertfordshire, Hatfield AL10 9AB, UK. E-mail: y.sun@herts.ac.uk.

Jiliang Zhang is with the College of Integrated Circuits, Hunan University, Changsha 410082, China. E-mail: zhangjiliang@hnu.edu.cn.

ticity, excitatory and inhibitory regulation, as well as intrinsic membrane properties. From a cellular structural perspective, membrane properties are the primary factors influencing signal firing rates [24]. The growth of myelin sheaths can alter membrane properties, thus affecting neural signal firing rates. In conclusion, myelin sheaths have the ability to influence the propagation speed of neural signals and the frequency of pulse firing. Therefore, the biological functionality of myelin sheaths should not be overlooked in research related to neuromorphic computing.

Artificial synapses and ion channels are often built with memristors for their low power consumption, ease of integration [25]–[27], nonlinearity [28]–[31], consumer electronics [32], [33]. Additionally, high-order memristors’ nonlinear properties are frequently utilized with capacitors to simulate the discharging characteristics of biological neurons [34]–[36]. Alternatively, referencing the Hodgkin-Huxley (HH) model, memristors and other components are employed to simulate the functions of ion channels, synapses, and other cellular organelles, thereby constructing neuronal circuits [37]–[40]. While both neuronal circuit designs, developed through different design approaches, have achieved considerable biomimetic characteristics, for lack of consideration of the function of the myelin sheath, they suffer from limitations such as fixed firing rates, fixed excitation thresholds, and fixed signal transmission speed. The growth of myelin sheaths accompanies the entire brain development process [41], which implies that the same neuron may exhibit different firing rates and signal conduction velocities at different stages. Incorporating myelin sheath function into neuronal circuit design will provide smarter and low-power design methods for the consumer electronics products.

However, few current neuromorphic networks consider myelin sheath function in artificial neurons, the regulation of neuronal firing rates is achieved indirectly by increasing stimulation and altering the connection strengths of artificial synapses, which is not conducive to forming stable and efficient neural circuits, making it difficult to establish “muscle memory”. Artificial neurons with fixed excitation conditions may not activate in deep networks due to signal attenuation or vanishing. This phenomenon is quite common in spiking neural networks [42].

Myelination growth can alter the activation conditions of neurons, making the neurons at the end of the neural circuit more prone to activation. Therefore, introducing myelination functionality into artificial neuronal circuits is crucial. This not only enhances the computational capabilities of individual artificial neurons but also strengthens the overall adaptability of artificial neural networks. Furthermore, it can also reduce the power consumption of neural circuitry. This paper studies the structure and biological characteristics of myelin sheaths and designs a biomimetic neuronal circuit system that incorporates myelin sheath functionality, providing a biological solution to the above issues.

The rest of this paper is organized as follows. Section II primarily discusses the essential biological background knowledge, mathematical models of ion channel memristors, voltage-controlled capacitors, and voltage-controlled resistors,

and the dynamical equations of ABNCS. Section III covers *PSpice* simulations, detailing the experimental schematics and the results and analysis of the simulation results. Section IV involves practical circuit experiments conducted to validate the effectiveness of simulating myelin sheath functionality using voltage-controlled capacitors and voltage-controlled resistors, as well as to demonstrate the adaptability of ABNCS through controlled variable components. Section V focuses on the applications of ABNCS. Coupling comparative experiments further validate ABNCS’s capability to adaptively modify neural circuit discharge frequency and speed, enhancing stimulus responsiveness. Additionally, it addresses the challenge of forward training in pulse neural networks. Section VI is the conclusion, summarizing the paper.

II. PRELIMINARY

In this section, we will provide a detailed introduction to the physiological structure and signal transmission mechanism of myelinated neurons. Additionally, we will also present mathematical models of memristors, variable capacitors, and other devices constituting various cellular components of neurons.

A. Biological structure of myelinated neurons

As shown in Fig. 2(a), the myelin sheath wraps around the surface of the axon, leaving sections of the axon exposed at regular intervals, forming the nodes of Ranvier. Unlike unmyelinated axons, myelinated axons do not have ion channels on the surface of the axonal cell membrane that is wrapped by the myelin sheath. Ionic exchange inside and outside the axon can only occur through ion channels on the cell membrane at the nodes of Ranvier. The physiological structure of myelinated neurons forms the basis for the saltatory propagation of neural signals.

B. The signal transmission mechanism of myelinated neurons

Neurons transmit signals by continuously altering the membrane potential of the axon. As shown in Fig. 2(c), the generation of APs leads to changes in the axon membrane potential, subsequently stimulating sodium and potassium ion channels in the direction of signal transmission to generate new APs, until the signal is transmitted to the axon terminal. As shown in Fig. 2(b), due to the myelin sheath wrapping, ion channels are only present at the nodes of Ranvier in the axon, where APs can be generated. Therefore, the signaling transmission in myelinated neurons occurs in a saltatory manner, and the transmission speed is exceptionally fast. Understood from the perspective of physical parameters, the ratio of the propagation speed v , spatial constant λ (also referred to as “characteristic length scale”), and time constant τ of neural signals is directly proportional, $v \propto \lambda/\tau$ [14], [43]–[45]. λ and τ are determined by Eq. (1) and Eq. (2) [46].

$$\lambda = \sqrt{\frac{r_T}{r_L}} = \sqrt{\frac{R_T \cdot d}{4 \cdot R_L}}, \quad (1)$$

$$\tau = R_T \cdot C, \quad (2)$$

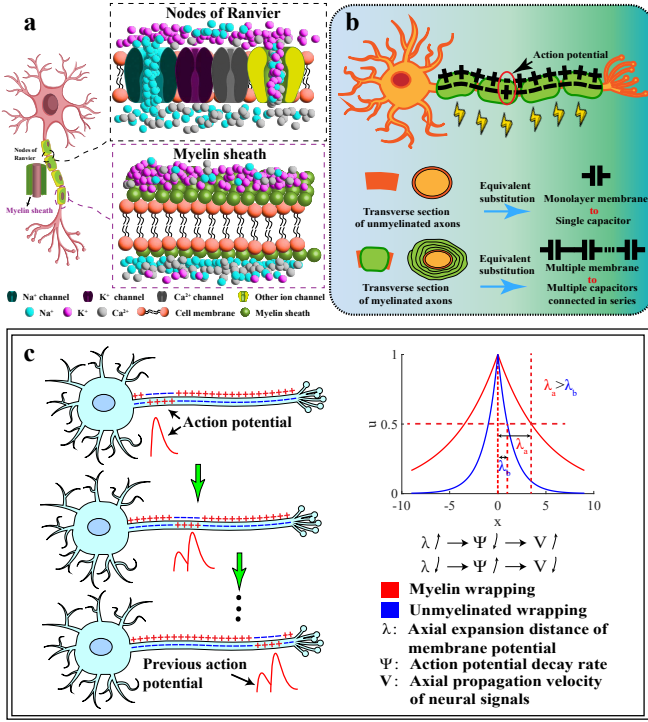


Fig. 2. (a) the physiological structure of myelin sheath; (b) Signal transmission mode of myelinated neurons; (c) Signal transmission mode of unmyelinated neurons.

where longitudinal and transversal resistors are denoted by R_L and R_T , r_L and r_T are the differentials of R_L and R_T , respectively. C represents the capacitance of the axonal cell membrane, and d is the diameter of the axon.

When the axon is wrapped by multiple layers of the myelin sheath, its effect is equivalent to multiple capacitors in series, as shown in Fig. 2(b), which leads to a rapid decrease in axonal capacitance C and an increase in membrane resistance R_T . According to Eq. (2), due to C decreasing faster than R_T increasing, the overall value of τ decreases, and the time for generating an AP is shorter. Ion channels are only present at the nodes of Ranvier, so when an AP is generated, ions within the axoplasm can only move along the axon and cannot freely exchange with extracellular ions. Furthermore, the AP will decay more slowly, resulting in larger spatial leaps, as depicted in Fig. 2(c). This significantly enhances the signal transmission speed. The same conclusion can also be derived from physical parameters. According to Eq. (1), myelination increases membrane resistance R_T and axon diameter d , leading to a larger spatial constant. This allows APs to travel further along the axon and neural signal.

C. Electronic device equivalent replacement for neurocellular organelles

From a cellular structure perspective, neurons are, in fact, high-order chaotic systems composed of various nonlinear organelles. If higher-order nonlinear devices are adopted for neuronal functionality in order to achieve greater integration, it is likely that certain biological characteristics and robustness

of neurons will be compromised. Therefore, we utilize various devices to simulate the functions of different organelles and refer to the HH model to construct a neuronal circuit system, to achieve more closely the biomimetic characteristics.

Ion channels are crucial cellular components for generating APs, and their characteristics are similar to those of high-speed memristors. Hence, we simulate ion channels by utilizing high-speed memristor models. Neurons generate APs in response to stimuli. APs are classified as either excitatory postsynaptic potentials (EPSPs) or inhibitory postsynaptic potentials (IPSPs) depending on the stimulus type. Na^+ , K^+ , and Ca^{2+} ion channels are involved in the generation of EPSP or IPSP [47]–[49]. Hence, we employ high-speed memristor models to simulate these three types of memristors. The Na^+ channels involved in generating APs possess characteristics of rapid activation and inactivation, with an activation threshold of approximately -55mV . K^+ and Ca^{2+} channels exhibit fast activation and slow inactivation characteristics, with activation thresholds of approximately 20mV and -80mV , respectively. The biological characteristics of Na^+ and Ca^{2+} channels are similar, thus requiring parameter adjustments to implement their functions using the same memristor model. The dynamic equation of this memristor model is described by Eq. (3), (4), and (5). Eq. (3) depicts the variation in memristor resistance, Eq. (4) describes the switching speed between high and low resistance states, and Eq. (5) characterizes the nonlinearity of the memristor.

$$V(t) = R_{off} - x \cdot \Delta R \cdot i(t), \quad (3)$$

$$\frac{dx}{dt} = \begin{cases} q_1 \cdot k_{on}^{b_1} \cdot f(x) \cdot i(t) \cdot \Delta R, & V(t) > V_{th1} \\ 0, & V_{th2} < V(t) \leq V_{th1} \\ q_2 \cdot k_{off}^{b_2} \cdot f(x) \cdot i(t) \cdot \Delta R, & V(t) \leq V_{th2}, \end{cases} \quad (4)$$

$$f(x) = a \cdot (1 + x)^p, \quad (5)$$

where $V(t)$ represents the voltage across the memristor's two terminals, R_{off} is the high resistance value of the memristor, and ΔR is the difference between the high resistance value R_{off} and the low resistance value R_{on} . The x is the resistance adjustment coefficient, $i(t)$ is the current passing through the memristor and $f(x)$ is the window function. The q_1 , q_2 , a_1 , a_2 , k_{off} , k_{on} , a , and p are all parameters. V_{th1} and V_{th2} represent the activation threshold and inactivation threshold, respectively.

Compared to Na^+ and Ca^{2+} channels, K^+ channels exhibit relatively unique inactivation characteristics, which requires the usage of a different memristor model. The dynamic equation of this memristor is described by Eq. (3), (5), and (6). The b_1 and b_2 are both parameters, in Eq. (6).

$$\frac{dx}{dt} = \begin{cases} q_1 \cdot k_{on}^{b_1} \cdot f(x) \cdot i(t) \cdot \Delta R, & V(t) > V_{th1} \\ 0, & V_{th1} \geq V(t) > V_{th2} \\ k_{off}^{b_2} \cdot f(x) \cdot i(t)^{q_2} \cdot \Delta R, & V(t) \leq V_{th2}. \end{cases} \quad (6)$$

Due to differences in ion concentrations inside and outside the neuron, a resting membrane potential is established.

Function of the cell membrane is akin to that of a capacitor. As shown in Fig. 2(b), a single layer of cell membrane is equivalent to a capacitor, and the growth of the myelin sheath leads to the stacking of multiple layers of membranes, which is equivalent to multiple capacitors connected in series. Process of myelin sheath growth is also known as myelination. Myelination alters membrane capacitance and membrane resistance to modify the firing frequency and speed of neurons.

Adaptive adjustment of membrane permeability and membrane capacitance is crucial for achieving myelin sheath functionality. We employ voltage-controlled variable resistors and variable capacitors to simulate myelination. With each discharge, there is a subtle adjustment of resistance and capacitance values, thereby regulating the firing frequency, speed, and activation conditions of biomimetic neurons, mimicking the process of neuronal myelin sheath growth. The dynamic equation of the voltage-controlled variable capacitor is jointly described by Eq. (7), (8), and (9). Eq. (8) is obtained by substituting Eq. (7) into $q = c \cdot v$, q represents charge, c is capacitance, and v stands for voltage. Eq. (7) describes the variation pattern of the variable capacitor's capacitance, while Eq. (9) characterizes the speed and nonlinearity of the variable capacitor's capacitance variation.

$$C(t) = \frac{1}{\frac{1}{C_{off}} + \frac{x_c \cdot k}{\Delta C}}, \quad (7)$$

$$V_c(t) = \frac{\int i_c(t) dt}{\frac{1}{C_{off}} + \frac{x_c \cdot k}{\Delta C}}, \quad (8)$$

$$\frac{dx}{dt} = \begin{cases} g \cdot n^m \cdot (1+x)^e, & V(t) > V_{th}^c \\ 0, & V(t) \leq V_{th}^c \end{cases}, \quad (9)$$

where, $C(t)$ is the real-time capacitance of the voltage-controlled variable capacitor, C_{off} is the initial capacitance, and ΔC is the capacitance associated with each layer of the myelin sheath. The $V_c(t)$ and $i_c(t)$ represent the voltage and current across the variable capacitor, respectively, while k denotes the number of myelin sheath layers. The x_c is the capacitance adjustment coefficient. The g , n , m , k , and e are parameters that control the rate of capacitance variation and nonlinearity. The V_{th}^c represents the triggering threshold. As for the voltage-controlled variable resistor, it is essentially a simplified memristor, and its dynamics can be fully described by Eq. (3), (5), and (10).

$$\frac{dx}{dt} = \begin{cases} q_1 \cdot k_{on}^{b_1} \cdot f(x) \cdot i(t) \cdot \Delta R, & V(t) > V_{th1} \\ 0, & V(t) \leq V_{th1} \end{cases}, \quad (10)$$

D. Dynamics of adaptive biomimetic neuronal circuit systems

Fig. 3 depicts the adaptive biomimetic neuronal circuit and the corresponding electronic components as cell organelles. As shown in Fig. 3(a), memristors R_{Na} , R_K , and R_{Ca} are used to simulate the functions of Na^+ , K^+ , and Ca^{2+} channels, while the variable capacitor $C_i (i = 1, 2, 3)$ is used to substitute for the biological functions of the cell membrane and myelin sheath. The variable resistor R_M is employed to

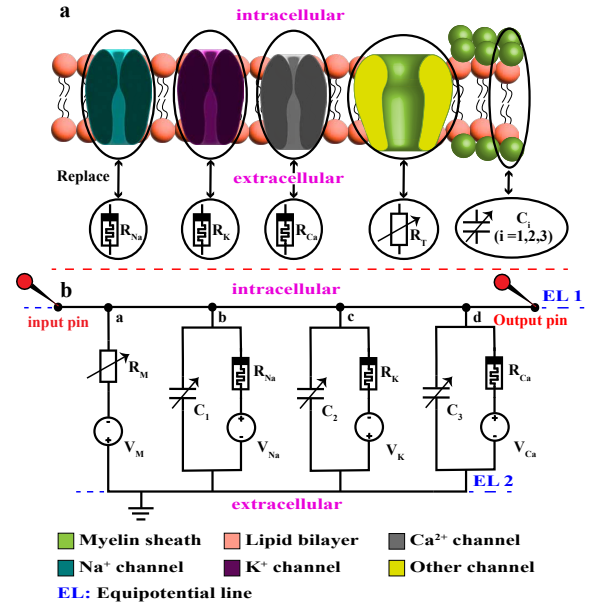


Fig. 3. (a) Corresponding electronic components as cell organelles; (b) Adaptive biomimetic neuronal circuits.

simulate the remaining non-voltage-gated, constitutively open ion channels while also simulating changes in cell membrane permeability caused by myelin sheath wrapping. The V_{Na} , V_K , and V_{Ca} represent the Nernst potentials generated by the concentration difference of sodium, potassium, and calcium ions inside and outside the neuron. The V_M is the Nernst potential generated by the concentration difference of the remaining ions, primarily functioning to regulate the potential difference between the inside and outside of the neuron to around $-71mV$.

The dynamic equations of the adaptive biomimetic neuronal circuit system are constructed according to Kirchhoff's laws. The conservation of electric charge on a piece of membrane implies that the applied current $I(t)$ may be split into a capacitive current I_C which charges the capacitor C and further components I_k which pass through the ion channels. Thus

$$I(t) = \sum_n I_c(t) + \sum_k I_k(t), \quad (11)$$

where the sum runs over all ion channels. From the definition of a capacity $C = q/u$ where q is a charge and u the voltage across the capacitor, we find the charging current $I_C = C \cdot du/dt$. Furthermore, the growth of the myelin sheath leads to changes in capacitance values, $I_C = dc \cdot du/d^2t$. Hence from Eq. (12).

$$\sum_n I_c(t) = \frac{(dc_1 + dc_2 + dc_3) \cdot du}{d^2t}, \quad (12)$$

where u represents the total Nernst potential generated by the concentration difference of ions inside and outside the cell, namely membrane potential, which is the potential difference between equipotential lines 1 and 2 in Fig. 3(b). The total charge leakage from all ion channels is described by Eq. (13).

TABLE I
 PARAMETERS OF ION CHANNEL MEMRISTORS.

| ID | Ion CH | R _{off} | R _{on} | V _{th1} | V _{th2} | a | b ₁ | b ₂ | p | k _{on} | q ₁ | q ₂ | Dynamical Eq. |
|----|---------------------|------------------|-----------------|------------------|------------------|---|----------------|----------------|-----|-----------------|----------------|----------------|----------------|
| 1 | Na ⁺ CH | 1MΩ | 200Ω | -110mV | -119.5mV | 1 | 15 | 2 | 4 | 2 | 1 | 1 | (3), (4), (5) |
| 2 | K ⁺ CH | 1MΩ | 20Ω | 97mV | 7mV | 1 | 18 | -9.8 | 4 | 2 | 1.05 | -0.51 | (3), (5), (6) |
| 3 | Ca ²⁺ CH | 1MΩ | 10kΩ | -195mV | -120mV | 1 | 7 | 5 | 1.2 | 2 | 1 | 1 | (3), (4), (5) |
| 4 | Other(M) CH | 10KΩ | 3kΩ | 10mV | - | 1 | 10 | - | 1.2 | - | 1 | - | (3), (4), (10) |

Note1 : In all memristors, the value of k_{off} is 2.

Note2 : The symbol '-' represents an empty value.

Note3 : $V_{Na} = 55mV$, $V_{Na} = -77mV$, $V_{Ca} = 122mV$, $V_M = -71mV$.

 TABLE II
 PARAMETERS OF VOLTAGE-CONTROLLED VARIABLE CAPACITOR.

| i | C _{off} | ΔC | V _{th} ^c | k | g | n | m | e | Dynamical Eq. |
|---|------------------|-----|------------------------------|---|---|---|-----|---|---------------|
| 1 | 3μF | 3μF | 10mV | 5 | 1 | 2 | 1.5 | 2 | (7), (8), (9) |
| 2 | 3μF | 3μF | 10mV | 5 | 1 | 2 | 1.5 | 2 | (7), (8), (9) |
| 3 | 3μF | 3μF | 10mV | 5 | 1 | 2 | 0.5 | 2 | (7), (8), (9) |

$$\sum_k I_k = g_{Na} \cdot (u - E_{Na}) + g_K \cdot (u - E_K) + g_{Ca} \cdot (u - E_{Ca}) + g_M \cdot (u - E_M). \quad (13)$$

Parameters g_{Na} , g_K , and g_{Ca} denote conductance of Na⁺, K⁺, and Ca²⁺ throughout the process of AP generation. The values of these variables are determined collectively by Eq. (3), (4), (5), (6), and (10). Conductance of leakage channel are represented by g_M . Parameters E_{Na} , E_K , E_{Ca} , and E_M are the reversal potentials. Parameters g_{Na} , g_K , g_{Ca} , and g_M are all determined by the respective ion channel's dynamic equations.

III. SIMULATION OF THE ADAPTIVE BIOMIMETIC NEURONAL CIRCUIT SYSTEM

In this section, we constructed circuit models on *PSpice* based on the dynamic equations of memristors, variable resistors, and variable capacitors mentioned in the previous section. Additionally, we built the adaptive biomimetic neuronal circuit system according to Fig. 3(b). It can be observed, either from the Eq. (11), (12) and (13) or from the circuit diagram in Fig. 3(b), that the ABNCS is a high-dimensional circuit system. For biological neurons, adding each type of ion channel requires introducing an additional set of variables to describe their microdynamics. Therefore, biological neurons are, in fact, more complex systems with higher dimensions. Hence, to attain more specific and comprehensive biomimetic characteristics, designing high-complexity neuronal circuit systems becomes inevitable.

The circuit for the simulation was constructed strictly according to Fig. 3(b), and the relevant parameters for the memristors, voltage-controlled variable resistors, and voltage-controlled variable capacitors used are listed in Tables I and II. The simulations were conducted using *PSpice* software. In the simulations, we applied continuous positive and negative current stimuli to the ABNCS, and the results are shown in Fig. 4. Analyzing Fig. 4(a) reveals that in the initial phase of continuous excitatory stimulation to the ABNCS, its firing

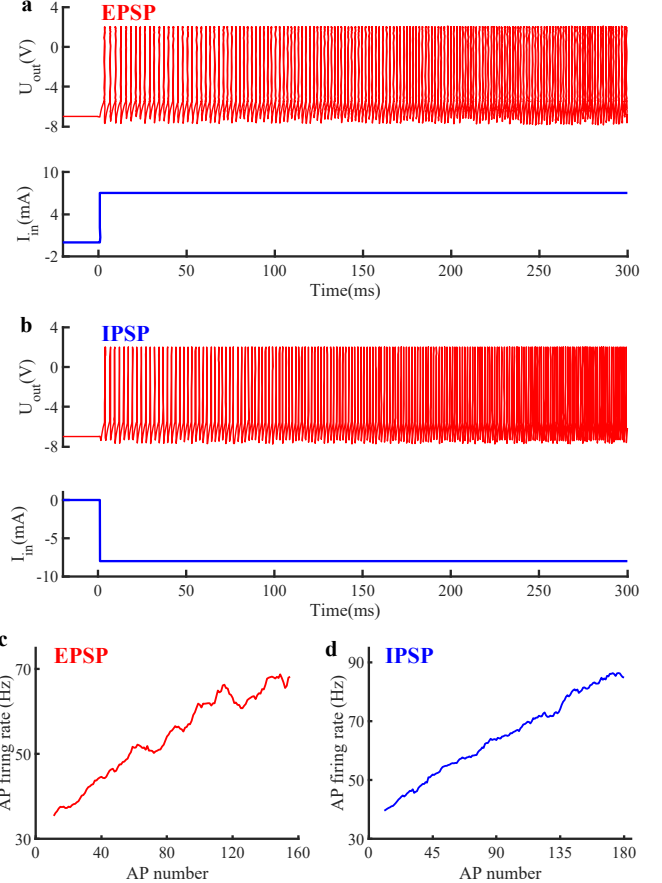


Fig. 4. Simulation results of the adaptive biomimetic neuronal circuit system. (a) The response of ABNCS to excitatory stimuli; (b) Response of ABNCS to inhibitory stimuli; (c) The relationship between the number of APs and ABNCS firing rate under excitatory stimulation; (d) The relationship between the number of APs and ABNCS firing rate under inhibitory stimulation.

rate is relatively low. With an increase in the number of APs, the ABNCS's firing rate gradually increases, indicating that the signal transmission speed accelerates accordingly. Observing Fig. 4(c), it can also be noted that as the number of APs generated by the ABNCS increases, the firing rate also significantly rises, indicating a linear relationship between the two. Inhibitory stimuli can also induce APs, leading to an increase in the ABNCS's firing rate, as shown in the Fig. 4(b). One noteworthy point is that, compared to excitatory stimuli, inhibitory stimuli of the same intensity have a greater impact on the ABNCS, resulting in a higher number of APs generated by the ABNCS within a unit of time. The increase

TABLE III
PERFORMANCE COMPARISON BETWEEN HH AND ABNCS.

| Model | | I_{in} | R_M | $C_i (i = 1, 2, 3)$ | Q | f |
|-------|---------|-----------|------------|---------------------|-----------|-----------|
| HH | Initial | $10\mu A$ | $3k\Omega$ | $3.5\mu F$ | $794.9nC$ | $24.69Hz$ |
| | Mature | $10\mu A$ | $3k\Omega$ | $3.5\mu F$ | $794.9nC$ | $24.69Hz$ |
| ABNCS | Initial | $10\mu A$ | $3k\Omega$ | $3.5\mu F$ | $794.9nC$ | $24.69Hz$ |
| | Mature | $10\mu A$ | $9k\Omega$ | $1.5\mu F$ | $289.9nC$ | $73.04Hz$ |

Note1 : I_{in} represents the magnitude of the input current; Q represents the amount of charge required to emit an AP; The f is the spike firing frequency.

in firing rate is more pronounced, as can be observed in Fig. 4(d). Comparing the ABNCS's responses to excitatory and inhibitory stimuli, it can be observed that the ABNCS exhibits different responses to different types and intensities of stimuli, similar to biological neurons.

Charge required and the firing frequency for a single spike emission in HH and ABNCS are presented in the Table III. energy consumption Q is calculated according to Eq. (14). From the Table. III, it is evident that in the initial stage, the fundamental parameters of HH and ABNCS are identical, with equivalent energy consumption and peak firing rates. However, after ABNCS emits a certain number of spikes, it undergoes growth, adaptively adjusting its parameters. As a result, the spike firing rate significantly increases while the energy consumption decreases substantially. HH lacks growth characteristics, so its properties remain consistent with the initial stage.

$$Q = \int_{t_1}^{t_2} I_M dt + n \cdot (V_P - V_R) \cdot C, \quad (14)$$

where, Q represents the amount of charge required to emit an AP. Interval (t_1, t_2) represents the time interval for emitting an AP. I_M is the current in branch 'a' in Fig. 3(b). V_P and V_R respectively represent the spike peak potential and resting potential. C is the capacitance of the capacitor, which is cell membrane substitute. The n represents the number of capacitors.

IV. HARDWARE EXPERIMENTS AND VERIFICATION

A. Experimental setup

In order to further investigate the reasons for changes in the ABNCS's firing rate and excitation difficulty and to validate the ABNCS's reliability, we conducted practical experiments using memristor circuits to replace memristors. Fig. 5 depicts the practical experimental setup and the substituting circuits for the three ion channel memristors. The ion channel memristors are designed based on bidirectional controllable silicon with connection-holding capability. Taking the sodium ion channel memristor circuit as shown in Fig. 5(b) as an example, when the voltage at the input and output terminals reaches the triggering threshold, power is supplied to the control terminal of the bidirectional controllable silicon, causing the bidirectional controllable silicon to conduct, and a continuous current flows through it. Due to the connection-holding characteristics of the bidirectional controllable silicon, even if the power supply to the control terminal is removed, the

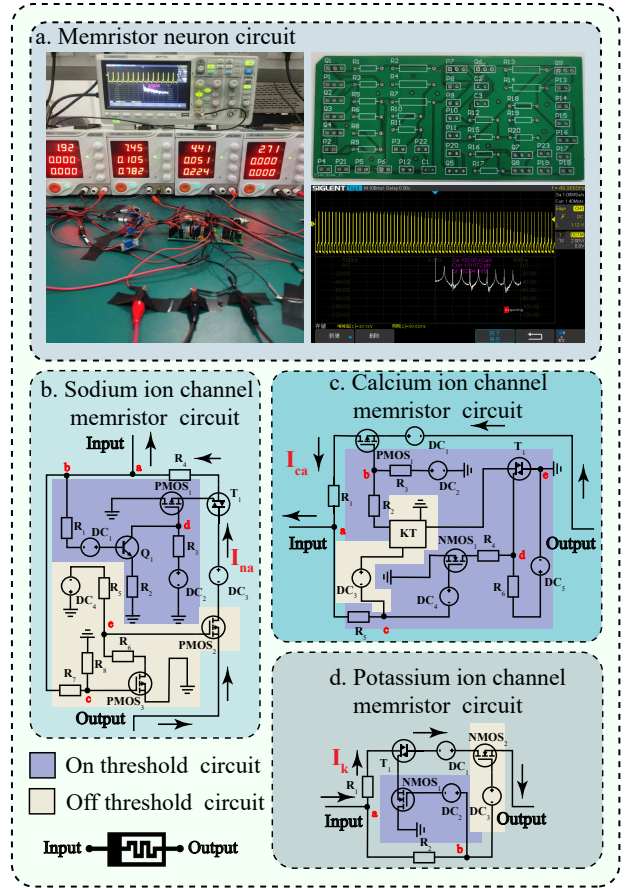


Fig. 5. Experimental setup and the corresponding memristor circuits for each ion channel. (a) Practical Experimental Scenarios and Some Experimental Results; (b) Sodium Ion Channel Memristor Circuit; (c) Calcium Ion Channel Memristor Circuit; (d) Potassium Ion Channel Memristor Circuit.

bidirectional controllable silicon can maintain its conducting state as long as the current passing through it does not approach zero or reverse. When the voltage at the input and output terminals reaches the shutdown threshold, the current flowing through the bidirectional controllable silicon is cut off by the MOSFET, thus preventing the bidirectional controllable silicon from conducting. The principles of the remaining two ion channel memristor circuits are similar to the sodium ion channel memristor circuit, and will not be further elaborated here. The parameters involved in all memristor circuits are shown in Table IV.

B. The impact of membrane permeability on firing characteristics

Analyzing Fig. 3(b), it can be observed that for charges within the ABNCS to flow to the outside of the ABNCS, they must pass through four pathways: a , b , c , and d . Adjusting the value of R_M in a pathways of Fig. 3(b) can effectively simulate changes in the permeability of neuronal cell membranes. The condition for the ABNCS to generate APs is that the voltage across $C_i (i = 1, 2, 3.)$ reaches the discharge threshold to trigger the ion channel memristor. Therefore, the charging time t of $C_i (i = 1, 2, 3.)$ is related to the firing rate, with shorter t resulting in a higher firing rate in a linear

TABLE IV
 PARAMETERS OF THE MEMRISTOR CIRCUIT.

| Category | R ₁ | R ₂ | R ₃ | R ₄ | R ₅ | R ₆ | R ₇ | R ₈ | DC ₁ | DC ₂ | DC ₃ | DC ₄ | DC ₅ |
|-----------------------------|----------------|----------------|----------------|----------------|----------------|----------------|----------------|----------------|-----------------|-----------------|-----------------|-----------------|-----------------|
| Na ⁺ CH circuit | 2MΩ | 0.1MΩ | 1MΩ | 0.2kΩ | 10kΩ | 1kΩ | 1.11MΩ | 0.39MΩ | 6.3V | 4V | 5.5V | 10V | - |
| K ⁺ CH circuit | 5Ω | 2MΩ | - | - | - | - | - | - | 7.7V | 2.5V | 9V | - | - |
| Ca ²⁺ CH circuit | 10kΩ | 10Ω | 100Ω | 10Ω | 2MΩ | 50Ω | - | - | 11.8V | 15V | 13V | 15V | 5V |

Note1 : The symbol '-' represents an empty value.
 Note2 : The KT stands for electromagnetic relay.

relationship between the two. To reduce the charging time t of the capacitor, efforts can be made from two aspects: increasing the value of R_M or decreasing the capacitance value of C_i ($i = 1, 2, 3$). From a physical formula perspective, this actually involves increasing the spatial constant λ or reducing the time parameter τ , as shown in Eq. (1) or (2).

In order to investigate the impact of the amount of charge flowing out of the system, namely Membrane permeability, on the ABNCS's discharge, we gradually increased the values of R_M in Fig. 3 and observed the ABNCS's output response. In practical experiments, the memristors in the ABNCS were all replaced by memristor circuits. Because it is easier to observe the impact of R_M variations on the ABNCS response under short current stimulation, we designed ABNCS with different R_M values and subjected them to fixed-duration short current stimuli. The experimental results are shown in Fig. 6. In Fig. 6 and 7, the value of the ABNCS's R_M is the same for each column, and the value of C_i ($i = 1, 2, 3$) is the same for each row, with $C_1 = C_2 = C_3$. Observing the first row of Fig. 6, namely Fig. 6(a), 6(b), 6(c), and 6(d), it can be noted that as R_M gradually increases, the duration of potential changes produced under the same stimulus also increases. The ABNCS requires more time to return to its initial state. The same conclusion can also be obtained from Eq. (1). According to Eq. (15), as R_M increases, R_T also increases, leading to an increase in the spatial constant. This implies that the changes in potential can propagate over a greater distance, hence resulting in an extended duration of potential changes.

$$R_T = \frac{1}{\frac{1}{R_M} + \frac{1}{R_{Na}} + \frac{1}{R_K} + \frac{1}{R_{Ca}}} \quad (15)$$

In addition, under the same stimulus intensity, compared to the ABNCS with a small R_M , the ABNCS with a larger R_M only requires a shorter stimulus duration to generate APs. This suggests that as R_M increases, the ABNCS becomes more active and is more prone to generating APs. As the capacitance C decreases, the ABNCS with high R is the first to initiate APs, and in some cases, it even triggers two APs under the same stimulus intensity. This phenomenon can be observed in Fig. 6. In an intuitive sense, as R_M increases, it is similar to a decrease in the permeability of the cell membrane. This restricts the flow of charge from inside the ABNCS to the outside, allowing more charge to accumulate for charging C_i ($i = 1, 2, 3$). This lowers the requirements for the ABNCS to generate APs.

It is important to note that R_M cannot increase indefinitely due to the permeability of the cell membrane. Excessively large R_M values can impede or interrupt the flow of charge

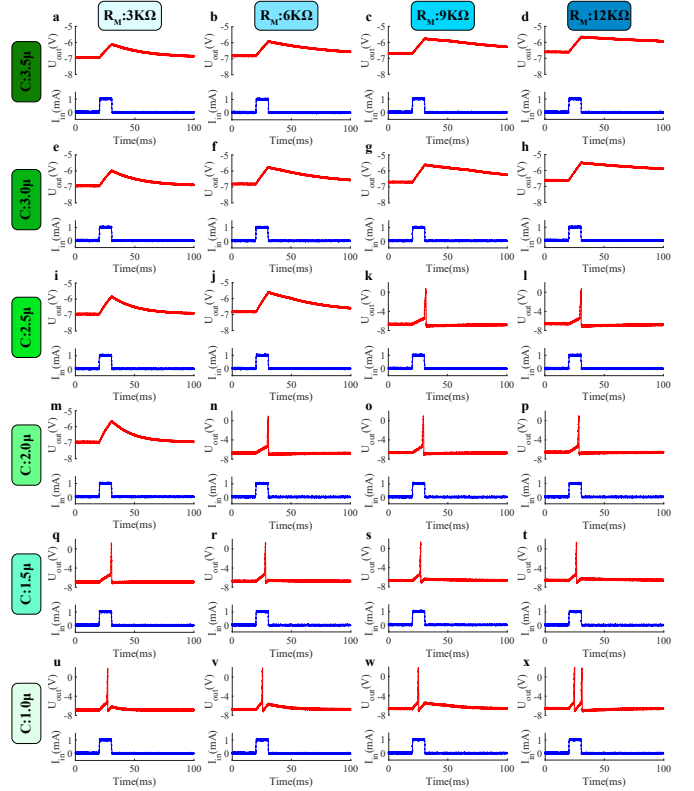


Fig. 6. The influence of changes in R_M and C_i ($i = 1, 2, 3$) on ABNCS response under short current stimulus.

across both ends of C_i ($i = 1, 2, 3$), causing the capacitor to charge too slowly or even preventing it from charging, and lead to an ABNCS failure. According to Eq. (2) and (15), it can also be inferred that excessively large R_M values will increase the time constant τ , prolonging the time required for the capacitor to charge.

However, if R_M is too small, a large amount of injected charge will flow into the ground node through branch 'a' in Fig. 3(b), which cannot effectively charge the capacitor, and lead to rapid discharge of the capacitor, reducing the space constant and diminishing the distance over which potential changes can propagate. Therefore, the variation of the R_M value must be set within an appropriate range to ensure the normal and efficient operation of the ABNCS. After repeated experiments, we have set the range of R_M variation to be $[3k\Omega, 10k\Omega]$. This range ensures that changes in R_M have a significant impact on the ABNCS's excitation while still maintaining normal ABNCS operation.

C. The influence of membrane capacitance on firing characteristics

The capacitance C_i ($i = 1, 2, 3$), namely neural cellmembrane capacitance, has a significant impact on the discharge rate and discharge speed of the ABNCS. Observing Fig. 6, it can be seen that as the capacitance value continues to decrease, even when R_M is very small, the ABNCS is still capable of generating APs. To further observe the impact of C_i ($i = 1, 2, 3$) variation on the ABNCS, we designed a new practical experiment with the same foundational setup as the previous one but utilized continuous current stimulation for the ABNCS.

The practical experimental results are shown in Fig. 7, it can be observed that as C_i ($i = 1, 2, 3$) decreases, the ABNCS's firing rate increases. The smaller the value of C_i ($i = 1, 2, 3$), the more pronounced the increase. Charging a capacitor follows the physical law $q = c \cdot v$, where q is the charge, c is the capacitance, and v is the voltage. A smaller capacitance implies that a smaller amount of charge is needed to quickly raise the voltage across the capacitor. Additionally, according to Eq. (2), as the capacitance decreases, the time constant decreases. This can effectively explain the phenomenon where decreasing capacitance leads to an increase in the ABNCS's firing rate. One important point to note is that in Fig. 7, as R gradually increases, the firing rate also shows a slight increase. This once again underscores that the signal propagation speed is jointly regulated by the time constant τ and the spatial constant λ , namely $v \propto \lambda/\tau$. An increase in R_M leads to an increase in R_T , subsequently resulting in an increase in the spatial constant λ , as indicated by Eq. (1). Although, according to Eq. (2), an increase in R_T leads to a decrease in the time constant τ , within a certain range, an increase in R_T still results in a higher ratio of spatial constant λ to time constant τ . This, in turn, leads to an increase in discharge rate and a faster signal transmission speed. This phenomenon further illustrates that the variation in the ABNCS's discharge rate is in line with the biological characteristics of neurons.

V. THE APPLICATION AND FUTURE OF THE ABNCS

A. Application of the ABNCS

To evaluate the performance of ABNCS in constructing neural networks, we designed coupled simulations. In the biological nervous system, information is transmitted between two neurons through synaptic connections. When the signal reaches the axon terminal, the presynaptic membrane releases neurotransmitters into the synaptic cleft, and receptors on the postsynaptic membrane of the next neuron receive the neurotransmitters and generate a response, completing the signal transmission.

Because of the unique structure and transmission mode of synapses, the signal transmission between neurons is discontinuous, with an approximate time interval of 6 milliseconds between neurons [50]. Currently, bio-inspired neural circuits primarily rely on artificial synapses for coupling. However, mainstream artificial synapses tend to focus on simulating synaptic plasticity while overlooking the unique signal delay transmission mechanism of biological synapses [51], [52]. In

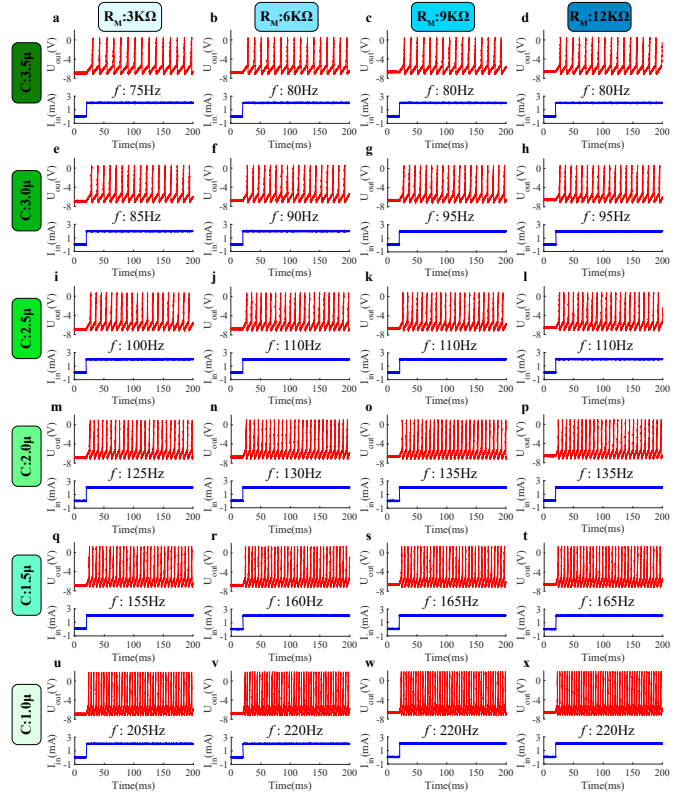


Fig. 7. The influence of changes in R_M and C_i ($i = 1, 2, 3$) on ABNCS response under prolonged current stimulus. The f is firing rate.

the biological nervous system, this intermittent signal transmission mode in the biological nervous system effectively prevents mutual interference between adjacent neurons. However, due to the continuous transmission of signals between neuronal circuits, employing artificial synapses for signal transmission inevitably leads to mutual interference between bio-inspired neural circuitry.

We employ RC circuits to simulate synaptic coupling. While the use of RC circuits as synapses results in continuous signal transmission, the charging of the capacitors introduces a certain degree of delay in signal propagation, which can mitigate mutual interference between neural circuits. Since our experimental focus is primarily on observing the plasticity of ABNCS itself, we construct RC circuits using conventional resistors and capacitors, rendering artificial synapses non-plastic, as shown in Fig. 8(a). Two sets of experiments are designed, one set involves coupling two HH model circuits, serving as the control group, while the other set involves coupling two ABNCS circuits, serving as the experimental group. The input and collection points of the signals are marked with pointers of different colors in Fig. 8(a).

The results of the two sets of experiments are shown in Fig. 8(b) and 8(c), with the colors of the pointers in Fig. 8(a) corresponding to the colors of the output result curves. To better assess whether the ability of the neural circuit to transmit signals can be modulated based on the number of pulses emitted by the circuit, we used short currents, long currents, and short currents of equal duration as inputs, as

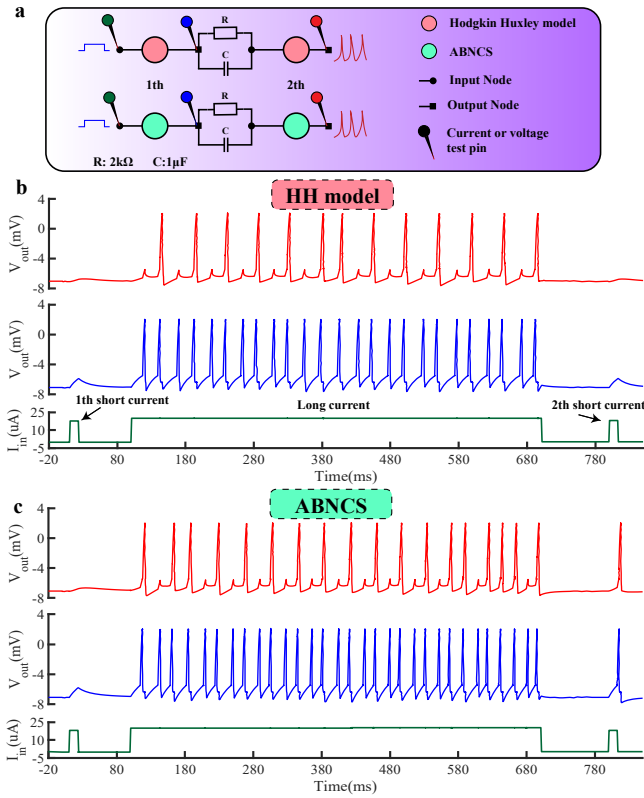


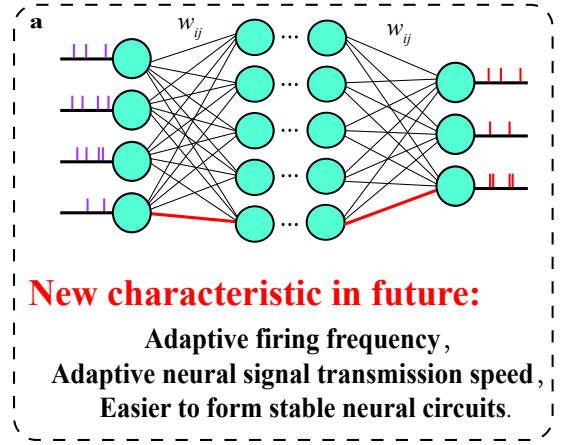
Fig. 8. Comparative experiments between HH model circuit and ABNCS. (a) Coupling comparative experiment circuit configuration; (b) Results of the coupling experiment of HH model circuits; (c) Results of the coupling experiment of ABNCS

shown in Fig. 8(b) and 8(c).

As shown in Fig. 8(b), in the neural circuit composed of the HH circuit model, the first short current did not trigger an AP, while the long current elicited a series of APs in the first and second neurons. Due to the factor of signal attenuation, the second neuron exhibited slightly fewer APs in response. The second short current also failed to elicit APs, and both neurons responded to it almost identically to the first short current. This indicates that the internal parameters of the neural circuit do not change with the quantity of transmitted signals.

In the second set of experiments, we replaced HH model with ABNCS while keeping all other settings identical to the first set. Observing Fig. 8(c), namely the red curve, it is evident that the firing frequency of the second neuron's APs increases as the number of APs rises, and the second short current also successfully triggered APs. This indicates that the neural circuit constructed using ABNCS is capable of adaptively adjusting its parameters with the increase in the number of APs, enhancing the circuit's responsiveness to the initial stimulus.

Higher vertebrates achieve specific actions by stimulating specific neural circuits. Repeatedly training a particular action by stimulating the corresponding neural circuit can lead to faster signal transmission along this circuit and an improvement in its responsiveness, resulting in what is known as muscle memory. Memory formation also occurs through



Beneficial for development

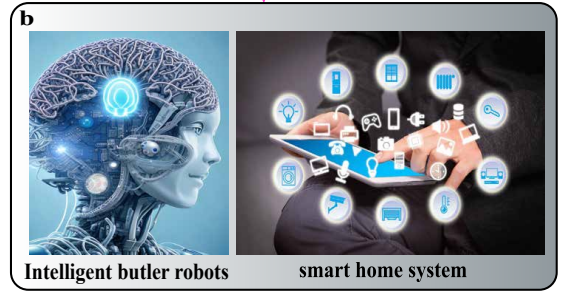


Fig. 9. Applications of ABNCS. (a) Characteristics of a Spiking Neural Network Constructed with ABNCS; (b) Conceptual diagram of an intelligent robot smart home system built with ABNCS.

similar mechanisms. While synaptic plasticity plays an important role in the processes mentioned above, synapses have little impact on the signal firing of neurons themselves. In contrast, myelin sheath growth can regulate the firing rate of neurons themselves, and when combined with synapses, it can form more stable neural circuits, greatly enhancing both signal transmission speed and efficiency. Therefore, ABNCS designed based on the characteristics of myelin sheath growth contribute to enhancing the signal transmission speed and efficiency of neural networks, thus simulating biological features akin to muscle memory. The comparative experiments depicted in Fig. 8 effectively validate this point.

B. Future of the ABNCS

As shown in Fig. 9(a), due to the biomimetic characteristics of ABNCS, spiking neural networks constructed using it can adaptively adjust firing rates, and signal transmission speed, form stable circuits, and enhance stimulus responsiveness. The spiking neural network constructed based on ABNCS relies on the number of APs to adjust parameters, and this method of modifying parameters belongs to feedforward regulation. This, to some extent, alleviates the challenge of conducting feedback training in spiking neural networks while expanding the training methods, thereby bringing the operational mechanism of spiking neural networks closer to that of the human brain. Furthermore, due to the adaptability of ABNCS,

it can lower the excitation threshold of artificial neural circuits, enabling effective training of neurons in deep spiking neural networks. The adaptability and growth potential of ABNCS makes it possible to develop intelligent butler robots and smart home systems with emotions, memories, associations, and consciousness, as illustrated in Fig. 9(b).

VI. CONCLUSION

This paper proposes a high firing rate and high signal transmission speed adaptive neuronal circuit system (ABNCS) based on myelin sheath functionality. First, ion channel memristors are constructed based on the biological characteristics of various ion channels involved in generating APs. Second, voltage-controlled variable capacitors and voltage-controlled variable resistors are employed to simulate myelin sheath growth while also substituting for the function of the cell membrane in isolating ions. Finally, ABNCS is constructed based on neuron structure. *PSpice* simulations and circuit experiments indicate that the firing frequency and signal transmission rate of ABNCS are linearly correlated with the number of APs, both in EPSP and EPSP. Neural circuit coupling comparative experiments demonstrate that neural circuits constructed with ABNCS do not need to rely on synaptic structures and can adjust the circuit's connection strength based on the number of APs, enhancing the stimulus responsiveness of the entire circuit. Therefore, the proposed ABNCS can effectively promote the research of high-speed, low-power biomimetic pulse neural networks and their applications in consumer electronics products. In our future work, biomimetic synapses will be researched to achieve a high-biomimetic pulse neural network.

REFERENCES

- [1] D. Javeed, M. S. Saeed, I. Ahmad, P. Kumar, A. Jolfaei, and M. Tahir, "An intelligent intrusion detection system for smart consumer electronics network," *IEEE Transactions on Consumer Electronics*, pp. 1–1, May. 2023.
- [2] M.-K. Yi, W.-K. Lee, and S. O. Hwang, "A human activity recognition method based on lightweight feature extraction combined with pruned and quantized cnn for wearable device," *IEEE Transactions on Consumer Electronics*, vol. 69, no. 3, pp. 657–670, Apr. 2023.
- [3] D. Kwon, S. Yun Woo, K.-H. Lee, J. Hwang, H. Kim, S.-H. Park, W. Shin, J.-H. Bae, J.-J. Kim, and J.-H. Lee, "Reconfigurable neuro-morphic computing block through integration of flash synapse arrays and super-steep neurons," *IEEE Transactions on Consumer Electronics*, vol. 9, no. 29, p. eadg9123, Jul. 2023.
- [4] J. Won, J. Kang, S. Hong, N. Han, M. Kang, Y. Park, Y. Roh, H. J. Seo, C. Joe, U. Cho, M. Kang, M. Um, K.-H. Lee, J.-E. Yang, M. Jung, H.-M. Lee, S. Oh, S. Kim, and S. Kim, "Device-algorithm co-optimization for an on-chip trainable capacitor-based synaptic device with igzo tft and retention-centric tiki-taka algorithm," *Advanced Science*, p. 2303018, Aug. 2023.
- [5] Z. Dong, X. Ji, C. S. Lai, and D. Qi, "Design and implementation of a flexible neuromorphic computing system for affective communication via memristive circuits," *IEEE Communications Magazine*, vol. 61, no. 1, pp. 74–80, 2023.
- [6] J. D. Sweatt, "Non-associative learning and memory," *Mechanisms of Memory (Second Edition)*, pp. 48–75, 2010.
- [7] A. Gidon, T. A. Zolnik, P. Fidzinski, F. Bolduan, A. Papoutsis, P. Poirazi, M. Holtkamp, I. Vida, and M. E. Larkum, "Dendritic action potentials and computation in human layer 2/3 cortical neurons," *Science*, vol. 367, no. 6473, pp. 83–87, Jan. 2020.
- [8] P. Liu, J.-L. Du, and C. He, "Developmental pruning of early-stage myelin segments during cns myelination in vivo," *Cell Res*, vol. 23, no. 7, pp. 962–4, Jul. 2013.
- [9] A. N. Hughes and B. Appel, "Microglia phagocytose myelin sheaths to modify developmental myelination," *Nat Neurosci*, vol. 23, no. 9, pp. 1055–1066, Sep. 2020.
- [10] J. H. Hines, A. M. Ravanelli, R. Schwandt, E. K. Scott, and B. Appel, "Neuronal activity biases axon selection for myelination in vivo," *Nat Neurosci*, vol. 18, no. 5, pp. 683–9, May. 2015.
- [11] S. Mensch, R. Almeida, T. Czopka, J. Ausborn, A. E. Manira, and D. A. Lyons, "Synaptic vesicle release regulates myelin sheath number of individual oligodendrocytes in vivo," *Nat Neurosci*, vol. 18, no. 5, p. 628–630, Apr. 2015.
- [12] E. M. Gibson, D. Purger, C. W. Mount, A. K. Goldstein, G. L. Lin, L. S. Wood, I. Inema, S. E. Miller, G. Bieri, J. B. Zuchero, B. A. Barres, P. J. Woo, H. Vogel, and M. Monje, "Neuronal activity promotes oligodendrogenesis and adaptive myelination in the mammalian brain," *Science*, vol. 344, no. 6183, p. 1252304, May. 2014.
- [13] S. Mitew, I. Gobius, L. R. Fenlon, S. J. McDougall, D. Hawkes, Y. L. Xing, H. Bujalka, A. L. Gundlach, L. J. Richards, T. J. Kilpatrick, T. D. Merson, and B. Emery, "Pharmacogenetic stimulation of neuronal activity increases myelination in an axon-specific manner," *Nat Commun*, vol. 9, no. 1, p. 306, Jan. 2018.
- [14] W. Gerstner, W. M. Kistler, R. Naud, and L. Paninski, *Neuronal Dynamics: From Single Neurons to Networks and Models of Cognition*. USA: Cambridge University Press, 2014.
- [15] D. Debanne, E. Campanac, A. Bialowas, E. Carlier, and G. Alcaraz, "Axon physiology," *Physiol Rev*, vol. 91, no. 2, pp. 555–602, Apr. 2011.
- [16] D. van Blooijns, M. A. van den Boom, J. F. van der Aar, G. M. Huiskamp, G. Castegnaro, M. Demuru, W. J. E. M. Zweiphenning, P. van Eijnsden, K. J. Miller, F. S. S. Leijten, and D. Hermes, "Developmental trajectory of transmission speed in the human brain," *Nat Neurosci*, vol. 541, no. 26, pp. 537–541, Mar. 2023.
- [17] G. Buzsáki, N. Logothetis, and W. Singer, "Scaling brain size, keeping timing: Evolutionary preservation of brain rhythms," *Neuron*, vol. 80, no. 3, pp. 751–764, Oct. 2023.
- [18] S. A. Neymotin, D. S. Daniels, B. Caldwell, R. A. McDougal, N. T. Carnevale, M. Jas, C. I. Moore, M. L. Hines, M. Hämmäläinen, and S. R. Jones, "Human neocortical neurosolver (hnn), a new software tool for interpreting the cellular and network origin of human meg/eeeg data," *Elife*, vol. 22, no. 9, p. e51214, Jan. 2020.
- [19] C. J. Honey, R. Kötter, M. Breakspear, and O. Sporns, "Network structure of cerebral cortex shapes functional connectivity on multiple time scales," *Proc Natl Acad Sci USA*, vol. 104, no. 24, pp. 10240–10245, Jun. 2007.
- [20] S. Li, D. W. McLaughlin, and D. Zhou, "Mathematical modeling and analysis of spatial neuron dynamics: Dendritic integration and beyond," *Communications on Pure and Applied Mathematics*, vol. 76, no. 1, pp. 114–162, Aug. 2021.
- [21] T. Akaishi, "New theoretical model of nerve conduction in unmyelinated nerves," *Front Physiol*, vol. 12, no. 8, p. 798, Oct. 2017.
- [22] M. Isokawa, "Membrane time constant as a tool to assess cell degeneration. brain res brain res protoc," *Front Physiol*, vol. 1, no. 2, pp. 114–116, May. 1997.
- [23] I. Tasaki, "The electro-saltatory transmission of the nerve impulse and the effect of narcosis upon the nerve fiber," *Am. J. Physiol*, vol. 127, no. 2, pp. 221–227, Aug. 1939.
- [24] A. F. Huxley and R. Stämpfli, "Evidence for saltatory conduction in peripheral myelinated nerve fibres," *J Physiol*, vol. 108, no. 3, pp. 315–339, May. 1949.
- [25] C. Leon, "If it's pinched it's a memristor," *Semiconductor Science and Technology*, vol. 29, no. 10, p. 104001, Sep. 2014.
- [26] Q. Hong, H. Chen, J. Sun, and C. Wang, "Memristive circuit implementation of a self-repairing network based on biological astrocytes in robot application," *IEEE Trans Neural Netw Learn Syst*, vol. 33, no. 5, pp. 2106–2120, May. 2022.
- [27] M. Jiang, J. Sun, C. Wang, Z. Liao, Y. Sun, Q. Hong, and J. Zhang, "An efficient memristive alternating crossbar array and the design of full adder," *Nonlinear Dynamics*, Sep. 2023.
- [28] H. Lin, C. Wang, F. Yu, Q. Hong, C. Xu, and Y. Sun, "A triple-memristor hopfield neural network with space multi-structure attractors and space initial-offset behaviors," *IEEE Transactions on Computer-Aided Design of Integrated Circuits and Systems*, Jun. 2023.
- [29] H. Lin, C. Wang, F. Yu, J. Sun, S. Du, Z. Deng, and Q. Deng, "A review of chaotic systems based on memristive hopfield neural networks," *Mathematics*, vol. 11, no. 6, p. 1369, Mar. 2023.
- [30] W. Yao, J. Liu, Y. Sun, J. Zhang, F. Yu, L. Cui, and H. Lin, "Dynamics analysis and image encryption application of hopfield neural network with a novel multistable and highly tunable memristor," *Nonlinear Dynamics*, 2023.

- [31] S. H. Sung, T. J. Kim, H. Shin, T. H. Im, and K. J. Lee, "Simultaneous emulation of synaptic and intrinsic plasticity using a memristive synapse," *Nature Communications*, vol. 13, no. 1, p. 2811, May. 2022.
- [32] Z. Dong, X. Ji, G. Zhou, M. Gao, and D. Qi, "Multimodal neuromorphic sensory-processing system with memristor circuits for smart home applications," *IEEE Transactions on Industry Applications*, vol. 59, no. 1, pp. 47–58, 2023.
- [33] Z. Dong, X. Ji, C. S. Lai, D. Qi, G. Zhou, and L. L. Lai, "Memristor-based hierarchical attention network for multimodal affective computing in mental health monitoring," *IEEE Consumer Electronics Magazine*, vol. 12, no. 4, pp. 94–106, 2023.
- [34] J. Ying, Y. Liang, G. Wang, P. Jin, L. Chen, and G. Chen, "Action potential and chaos near the edge of chaos in memristive circuits," *Chaos*, vol. 32, no. 9, p. 093101, Sep. 2022.
- [35] Y. Liang, G. Wang, G. Chen, Y. Dong, D. Yu, and H. H.-C. Iu, "S-type locally active memristor-based periodic and chaotic oscillators," *IEEE Transactions on Circuits and Systems I: Regular Papers*, vol. 67, no. 12, pp. 5139–5152, 2020.
- [36] Y. Liang, Q. Zhu, G. Wang, S. K. Nath, H. H.-C. Iu, S. K. Nandi, and R. G. Elliman, "Universal dynamics analysis of locally-active memristors and its applications," *IEEE Transactions on Circuits and Systems I: Regular Papers*, vol. 69, no. 3, pp. 1278–1290, 2022.
- [37] W. Yi, K. K. Tsang, S. K. Lam, X. Bai, J. A. Crowell, and E. A. Flores, "Biological plausibility and stochasticity in scalable vo2 active memristor neurons," *Nat Commun*, vol. 9, no. 1, p. 4661, Nov. 2018.
- [38] M.-R. G. Pickett, M. D. and R. S. Williams, "A scalable neuristor built with mott memristors," *Nat Mater*, vol. 12, no. 2, pp. 114–117, Feb. 2013.
- [39] H. M. Huang, R. Yang, Z. H. Tan, H. K. He, W. Zhou, J. Xiong, and X. Guo, "Quasi-hodgkin-huxley neurons with leaky integrate-and-fire functions physically realized with memristive devices," *Adv Mater*, vol. 31, no. 3, p. e1803849, Nov 2020.
- [40] G. Zhou, X. Ji, J. Li, F. Zhou, Z. Dong, B. Yan, B. Sun, W. Wang, X. Hu, Q. Song, L. Wang, and S. Duan, "Second-order associative memory circuit hardware implemented by the evolution from battery-like capacitance to resistive switching memory," *iScience*, vol. 25, no. 10, p. 105240, Sep 2022.
- [41] P. Tomáš, "Growth of white matter in the adolescent brain: Myelin or axon?" *Brain and Cognition*, vol. 72, no. 1, pp. 26–35, Feb. 2010.
- [42] P. U. Diehl, D. Neil, J. Binas, M. Cook, S.-C. Liu, and M. Pfeiffer, "Fast-classifying, high-accuracy spiking deep networks through weight and threshold balancing," in *International Joint Conference on Neural Networks (IJCNN), Killarney, Ireland, 2015*, pp. 1–8.
- [43] S. Binczak, J. C. Eilbeck, and A. C. Scott, "Ephaptic coupling of myelinated nerve fibers," *Physica D: Nonlinear Phenomena*, vol. 148, no. 1, pp. 159–174, Jan. 2001.
- [44] T. Erneux and G. Nicolis, "Propagating waves in discrete bistable reaction-diffusion systems," *Physica D: Nonlinear Phenomena*, vol. 67, no. 1, pp. 237–244, Aug. 1993.
- [45] S. G. Waxman, "Determinants of conduction velocity in myelinated nerve fibers," *Musc. Nerve*, vol. 3, no. 2, pp. 141–150, Mar. 1980.
- [46] M. Beierlein, *Determinants of conduction velocity in myelinated nerve fibers*, third edition ed. Boston: Academic Press, 2014.
- [47] C. D. Aizenman and D. J. Linden, "Regulation of the rebound depolarization and spontaneous firing patterns of deep nuclear neurons in slices of rat cerebellum," *J Neurophysiol*, vol. 82, no. 4, pp. 1697–709, Oct. 1999.
- [48] A. L. Blatz and K. L. Magleby, "Single apamin-blocked ca-activated k+ channels of small conductance in cultured rat skeletal muscle," *Nature*, vol. 323, no. 6090, pp. 718–20, Oct. 1986.
- [49] T. K and N. B., "Biophysics and structure-function relationship of t-type ca2+ channels," *Cell Calcium*, vol. 40, no. 2, pp. 97–114, Aug. 2006.
- [50] H. Markram, J. Lübke, M. Frotscher, A. Roth, and B. Sakmann, "Physiology and anatomy of synaptic connections between thick tufted pyramidal neurones in the developing rat neocortex," *J Physiol*, vol. 500, no. 2, pp. 409–40, Apr. 1997.
- [51] C. Wang, G.-Q. Mao, M. Huang, E. Huang, Z. Zhang, J. Yuan, W. Cheng, K.-H. Xue, X. Wang, and X. Miao, "Hfox/alloy superlattice-like memristive synapse," *Advanced Science*, vol. 9, no. 21, p. 2201446, May. 2022.
- [52] J. Zeng, J. Zhao, T. Bu, G. Liu, Y. Qi, H. Zhou, S. Dong, and C. Zhang, "A flexible tribotronic artificial synapse with bioinspired neurosensory behavior," *Nano-Micro Letters*, vol. 15, no. 1, p. 18, Dec. 2022.



interests include cognitive neuroscience, memristive logic circuits, and neuromorphic networks.



Jingru Sun graduated from Hunan University, China, in 2014 with a Ph.D. degree in computer science and technology. She is an associate professor in College of Computer Science and Electronic Engineering, Hunan University, Changsha, 410082, and Chongqing Research Institute, Hunan University, Chongqing 401120, China. She has published more than 30 papers and her research interests include memristive neural networks, brain-like computing, and intelligent transportation.



Wenjing Ma received the B.S. degree in engineering from Ocean University of China in 2022. She is currently pursuing the M.S. degree with the College of Computer Science and Electronic Engineering, Hunan University, Changsha, China. Her current research interests are memristors and brain-like computing.



Yichuang Sun (M'90-SM'99) received the B.Sc. and M.Sc. degrees from Dalian Maritime University, Dalian, China, in 1982 and 1985, respectively, and the Ph.D. degree from the University of York, York, U.K., in 1996, all in communications and electronics engineering. He is currently a Professor of Communications and Electronics, Head of Communications and Intelligent Systems Research Group, and Head of Electronic and Electrical Engineering at the University of Hertfordshire, UK. Professor Sun's expertise and interests are uniquely in the integration of electronics, communications and computing. He has been conducting active research in wireless and mobile communications, 5G and 6G technologies, RF systems and circuits, analogue and mixed-signal circuits, memristor circuits and systems, neural networks, machine learning, and neuromorphic computing. He has published some 400 papers in peer reviewed journals and conferences and contributed 10 chapters in edited research books. He has also published 4 texts and research books. Professor Sun serves on several Technical Committees of IEEE Circuits & Systems Society and IEEE Communications Society. He has been/is Book Series Editor of an IEE book series, Editor of 8 IEEE and international journals, and sole or lead Guest Editor of over 10 IEEE and IEE/IET journal special issues. He has been on the technical/scientific programme committee of numerous IEEE and international conferences in various roles. Professor Sun has been awarded many national and international awards, prizes, and honours.



Chunhua Wang received the M.S. degree from Zhengzhou University, Zhengzhou, China, in 1994, and the Ph.D. degree from Beijing University of Technology, Beijing, China, in 2003. He is currently a Professor of n 2019. He is currently an Associate Professor with College of computer science and electronic engineering Hunan University, Changsha, China. He is a Doctor tutor, Director of Advanced Communication Technology Key Laboratory of Hunan Universities, a member of Academic Committee of Hunan University, a Director of Chaos and Non-

linear Circuit Professional Committee of Circuit and System Branch of China Electronic Society. Now, his research interests include memristor circuit, complex networks, chaotic circuit, chaos secure communication, current-mode circuit and neural networks based on memristor. He has presided over 8 national and provincial projects, and published more than 120 papers, among which more than 100 were retrieved by SCI.



Jiliang Zhang received the Ph.D. degree in Computer Science and Technology from Hunan University, Changsha, China in 2015. From 2013 to 2014, he worked as a Research Scholar at the Maryland Embedded Systems and Hardware Security Lab, University of Maryland, College Park. From 2015 to 2017, he was an Associate Professor with Northeastern University, China. In April 2017, he joined the Hunan University. He is currently a Full Professor at the College of Integrated Circuits, Hunan University. He is Vice Dean of the College of Integrated Circuits

at Hunan University, the Director of Chip Security Institute of Hunan University, and the Secretary-General of CCF Fault Tolerant Computing Professional Committee. His current research interests include Hardware Security, Integrated Circuit Design and Intelligent System. He has authored more than 60 technical papers in leading journals and conferences. He was the recipient of CCF Integrated Circuit Early Career Award and the winner of Excellent Youth Fund of the National Natural Science Foundation of China. He is serving as a steering member for Hardware Security Forum of China. He is a senior member of IEEE/CCF.